Universal Long-Range Nanometric Bending of Water by Light

Gopal Verma and Kamal P. Singh
Department of Physical Sciences, Indian Institute of Science Education and Research Mohali, Sector-81, Manauli 140306, India
(Received 19 May 2015; published 2 October 2015)

Resolving mechanical effects of light on fluids has fundamental importance with wide applications. Most experiments to date on optofluidic interface deformation exploited radiation forces exerted by normally incident lasers. However, the intriguing effects of photon momentum for any configuration, including the unique total internal reflection regime, where an evanescent wave leaks above the interface, remain largely unexplored. A major difficulty in resolving nanomechanical effects has been the lack of a sensitive detection technique. Here, we devise a simple setup whereby a probe laser produces high-contrast Newton-ring-like fringes from a sessile water drop. The mechanical action of the photon momentum of a pump beam modulates the fringes, thus allowing us to perform a direct noninvasive measurement of a nanometric bulge with sub-5-nm precision. Remarkably, a < 10 nm difference in the height of the bulge due to different laser polarizations and nonlinear enhancement in the bulge near total internal reflection is isolated. In addition, the nanometric bulge is shown to extend far longer, 100 times beyond the pump spot. Our high precision data validate the century-old Minkowski theory for a general angle and offer potential for novel optofluidic devices and noncontact nanomanipulation strategies.

DOI: 10.1103/PhysRevLett.115.143902 PACS numbers: 42.25.Gy, 42.50.Wk, 68.03.-g, 83.85.Ei

Precision measurements of light-induced tiny deformations of an air-water (AW) interface are fundamental to unveil the nature of radiation forces with potential applications in optofluidics [1,2], reconfigurable lenses [1,3], micromanipulation of fluids [4,5], and fluid droplets [6]. In a pioneering experiment, Ashkin and Dziedzic observed an outward μm size bump on a free air-water interface using kW laser pulses [7]. The optical deformability of fluid interfaces has been used as a test bed for a long-standing debate on the Abraham-Minkowski formalism for photon momentum in a dielectric medium [8–14]. On the other hand, the interface deformation was much enhanced on fluid-fluid critical interfaces due to their much lower surface tension. The large interface deformation of such interfaces induced by sub-watt cw lasers demonstrated universal linear as well as nonlinear morphology of interfaces [15–17]. Most of these experiments provided key insight into the radiation forces in the simple case of normally incident lasers [7,17,18].

However, nanomechanical effects of photon momentum in the general case of any angle, in particular, close to the critical angle, remain largely unexplored. The total internal reflection (TIR) regime possesses unique properties, such as leaking of an evanescent wave above the interface and a small sideways displacement of the beam known as the Goos-Hänchen shift [19]. In addition, the magnitude of the radiation pressure weakly depends on incident polarization due to reflection from the interface caused by refractive index discontinuity. The intriguing radiation pressure effect near TIR has eluded experimental observation [20–24]. One of the major difficulties has been the lack of a sensitive detection technique to resolve nanometric deformation without any thermal side effects. High precision measurements may also test the validity of the century-old Minkowski formalism, which will have wide implications.

Here we use a pump-probe setup to demonstrate a universal nanometric bulge on a sessile water drop by photon momentum transfer near TIR. Using a noninvasive interferometric probe with < 5 nm precision, we unambiguously determined the direction, magnitude, and incidence angle dependence of the nanometric bulge. Remarkably, we isolated few nm differences in the bulge height for different polarizations along with enhanced deformation near TIR. In addition, the nanometric bulge is capillarylike and extended 100 times beyond the pump spot. Our high precision data validate Minkowski's corpuscular theory for any angle and offer the potential for wide applications.

A schematic diagram of our setup is shown in Fig. 1. The key idea behind our interferometric detection is to obtain high-contrast Newton-ring-like circular fringes from an air-water interface. For this, we placed a sessile water drop on a horizontal surface of a glass prism. A low power He-Ne laser, serving as a probe beam, entered at the center of the water drop quasinormally from above. The central thickness of the drop was below 1 mm, with typical diameter around 15 mm. While most of the probe beam was transmitted through the drop, we overlapped two partial reflections from the air-water and water-glass interfaces on a screen. Notably, these Fresnel reflections were of comparable intensities ($\approx$4%) for our glass prism. Their interference produces a stable, high-contrast Newton-ring-like fringe on the screen [insets in Fig. 2(a)].

The fringes obtained from the water drop are dynamic due to its natural evaporation [25]. The evaporation reduced

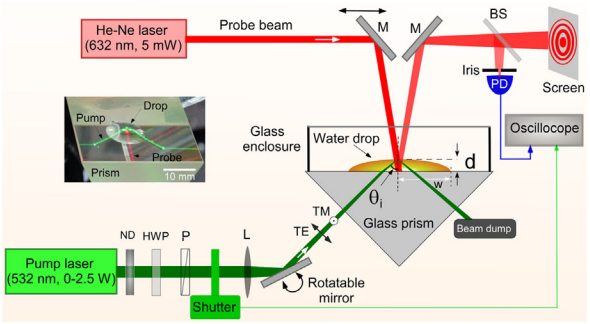

FIG. 1 (color online). Schematics of the experimental setup. A collimated He-Ne probe beam ($\lambda = 632$ nm, 5 mW) enters the sessile water drop quasinormally from above. A green pump beam is focused on the air-water interface from below at an angle θ_i. The probe beam transmitted through the drop is not shown. A photodiode (PD) simultaneously captured $I(t)$ of the central fringe (at the cross hair). Inset: Picture of the water drop. The probe beam was spatially overlapped by translating mirror (M). Neutral density filter (ND), half-wave plate (HWP), polarizer (P), lens (L), flat mirror (M).

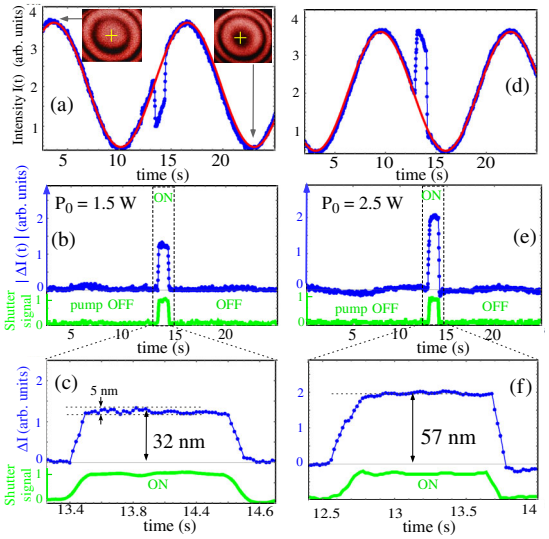

FIG. 2 (color online). Probe intensity $I(t)$ versus time for pump on-off cycles for $P_0 = 1.5$ W (left-hand column) and $P_0 = 2.5$ W (right-hand column). The solid red line in (a) and (d) is a $I_0 \cos^2[\alpha_0 d(t)]$ fit to the experimental data (blue circles) corresponding to natural evaporation rate ~18 nm/s. Two snapshots of the interference pattern (> 90% contrast) corresponding to minimum and maximum of $I(t)$ are shown in the insets of (a). Probe intensity data after subtracting evaporating baseline $\Delta I(t)$ for (b) $P_0 = 1.5$ W and (e) 2.5 W. The simultaneously recorded shutter signals controlling pump on and off are also shown. (c), (f) Zooms of $\Delta I(t)$ near pump on-off cycle. The corresponding elevation heights $h(r = 0)$ are labeled.

its central thickness $d(t)$, thereby introducing a time-dependent relative phase shift $\Delta\phi(t)$ between the interfering beams. In our case, the probe laser was quasinormal (incidence angle $< 5°$) to the interface. One can obtain $\Delta\phi(t) \simeq \alpha_0 d(t)$, where $\alpha_0 = 4\pi n_l/\lambda$ is a constant that only depends on the refractive index n_l of water and the wavelength λ of the probe. The resulting intensity, say, for the central fringe, was modulated in time as $I(t) = I_0 \cos^2[\alpha_0 d(t)]$ (see Fig. 2, top panels), where I_0 is the maximum intensity.

Importantly, the dynamic interference pattern is self-calibrating for nanoscale measurements. One fringe collapse, i.e., the central maximum to the next minimum of $I(t)$, corresponded to an optical path length change, $\lambda/4n_l \approx$ 117 nm, in our setup. We resolved 25 levels between the maximum and minimum of the intensity variation, using a photodiode (see Fig. 1), to achieve $117/25 \sim 5$ nm precision. Note that the accuracy of our technique is limited only by the resolution of the intensity detection aparatus and experimental noise floor. The nanometric precision and ease of our technique are ideal for direct measurement of the small pump laser-induced deformation of the AW interface of the water drop. To keep the interface almost static during typical pump exposure times (~1 s), we cover the water drop by a transparent enclosure that reduced the evaporation rate.

The slow evaporation of the water drop produces a linear reduction in its thickness. This can be used as a reference to determine the direction of the pump-induced deformation. Upon the pump laser irradiation (shutter open), if the photon momentum transfer causes the AW interface to rise (fall), the resulting phase shift in the evolution of the fringes will be opposite (in the same direction) to the one produced by the evaporation.

We first determine the direction of deformation. For this, we incident the pump beam on an AW interface at an angle of incidence $\theta_i = 49°$, which is above the critical angle ($\theta_c = 48.75°$). The TIR at the AW interface was further confirmed by the extinguished refracted beam above the drop, as well as by verifying almost unity throughput for $\theta_i \geq \theta_c$. In Figs. 2(a) and 2(d) we plot the intensity $I(t)$ as a function of time recorded with 1.5 and 2.5 W pump powers, respectively. Switching the pump beam on reverses the evolution of the probe intensity $I(t)$ as shown by the leading edge of the jumps in Figs. 2(a) and 2(d). Upon switching off the $I(t)$ jumps back to follow the sinusoidal curve due to evaporation, as seen by the trailing edge of the jumps (see video in Supplemental Material for two pump on-off events [26]). This unambiguously demonstrates that the pump beam induces an increase in the height of the AW interface corresponding to an outward bulge towards air.

By subtracting the evaporation baseline [red curves in Figs. 2(a) and 2(d)] from the original data, one can isolate the dynamics induced by the switching on or off of the pump beam (as shown in the middle panels in Fig. 2). Zooming in on the opening or closing time of the shutter [Figs. 2(c) and 2(f)] shows that the AW interface adiabatically followed the pump beam as shown by approximately the same rise or fall times for the blue and green curves. After background subtraction, the intensity $\Delta I(t)$ saturated

during 1 s exposure of the pump for both pump powers. The magnitude of the height variation corresponded to 32 and 57 nm (within 5 nm) for 1.5 and 2.5 W, respectively. The baseline fluctuations due to experimental noise were below 5 nm, which was used to assign error bars on the experimental data.

It is important to emphasize that our technique is nondestructive in the sense that the pump beam caused negligible thermal effect at the nanometric scale. This was demonstrated by good quality fits of our data with a single sinusoidal curve [red curves in Figs. 2(a) and 2(d)] before and after the pump exposure for both pump powers. This showed that the evaporation rate of the water drop remained unchanged ($\sim$18 nm/s) in spite of the pump exposure. In addition, the slope of the data and the fit curve during pump irradiation are almost identical. The negligible light-induced heating was also evident by almost zero baselines of $\Delta I(t)$ for the entire duration in Figs. 2(b) and 2(e). This quantitatively confirmed that the elevation of the interface is solely due to radiation pressure force.

The high precision of our experiment offers a unique opportunity to rigorously test the Minkowski theory in the general case of any incidence angle. Following the Minkowski formalism, the radiation pressure of a Gaussian laser beam obliquely incident at the AW interface from water is given by [15]

$$\Pi(\theta_i, r) = \frac{n_l I(r)}{c} f(\theta_i). \quad (1)$$

Here, $f(\theta_i) = \cos^2\theta_i[1 + R - (\tan\theta_i/\tan\theta_t)T]$ and c is the speed of light. θ_i and θ_t denote angles of incidence and transmission, respectively. The laser intensity is given by $I(r) = 2P_0/\pi w_0^2 \exp(-2r^2/w_0^2)$, where P_0 is the total power and w_0 is the beam waist at the focus. The coefficients of reflection $R(\theta_i, \theta_t)$ and transmission $T(\theta_i, \theta_t)$ are polarization dependent and follow $R + T = 1$. In the case of TIR, $R = 1$ for both TE and TM polarization (see Fig. 1). To generate a stationary deformation of the AW interface, the radiation pressure is balanced by both buoyancy and Laplace pressure. It leads to $\rho g h(\theta_i, r) - \gamma\kappa(r) = \Pi(\theta_i, r)$, where ρ is the density of water, γ is the surface tension, and $\kappa(r)$ is the curvature of the interface.

The solution of the above equation in cylindrical coordinates for the maximum deformation height leads to [15,27]

$$h(\theta_i, r) = \frac{P_0 n_l}{2\pi c} f(\theta_i) L(r), \quad (2)$$

where the spatial dependence is governed by the integral, $L(r) = \int_0^\infty [kJ_0(kr)e^{-w_0^2k^2/8}/(\gamma k^2 + \rho g)]dk$, and J_0 is the zeroth-order Bessel function. Several experiments tested the above model in the standard case of normal incidence ($\theta_i = 0$) [7,15,17,18]. However, near the TIR regime several interesting predictions of radiation pressure effects have eluded quantitative experimental tests so far. For example, the photon-momentum-induced deformation has nanometric sensitivity to the pump polarization and a long-range capillarylike spatial profile of the bulge.

In Fig. 3(a), we measured the bulge height $h(r = 0)$ versus the pump power in the TIR configuration ($\theta_i = 49°$) for two different values of the surface tension which was reduced using Sodium Dodecyl Sulphate (SDS) following Ref. [27]. The bulge height was averaged over five shots of the shutter opening for each power. A linear dependence on power was observed. It was in very good quantitative agreement with the deformation height given by Eq. (2) without any free-fitting parameter. Remarkably, here a few nm interface deformation produced by a low power $\sim$100 mW laser beam was clearly detected due to the high sensitivity of our technique.

By varying the incidence angle near the critical angle θ_c, we observed a nonlinear enhancement in the bulge height. Figure 3(b) shows our measurement of $h(r = 0)$ within $\pm 1°$ around θ_c for $P_0 = 2.5$ W. As θ_i approached the critical angle from below, a nonlinear threefold enhancement in the bulge height was observed when compared to the normally incident beam. In the TIR ($\theta_i > \theta_c$), the enhanced bulge varied slowly with θ_i. This is further illustrated by the right-hand side axis in Fig. 3(b), where we plotted a factor of enhancement in the radiation pressure $[\Pi(\theta_i)/\Pi(\theta_i = 0)]$. The threefold enhancement in the

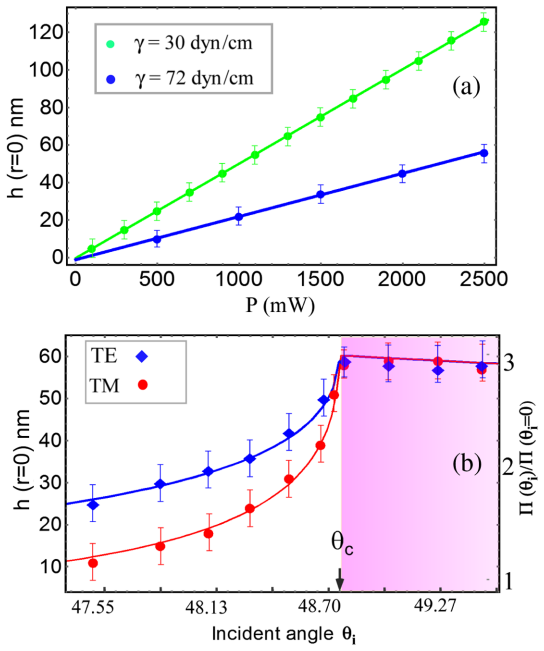

FIG. 3 (color online). (a) Bulge height $h(r = 0)$ versus the pump power P_0 in TIR regime ($\theta_i = 49°$). (b) The bulge height $h(r = 0)$ versus θ_i measured within $\pm 1°$ of θ_c. The data are shown for both TE and TM polarizations at $P_0 = 2.5$ W. Solid lines are fits with Eq. (2). The right-hand axis on (b) plots enhancement in the radiation pressure when compared to $\theta_i = 0°$. Error bars denote the experimental precision. Pump spot size was $2w_0 \simeq 40$ μm.

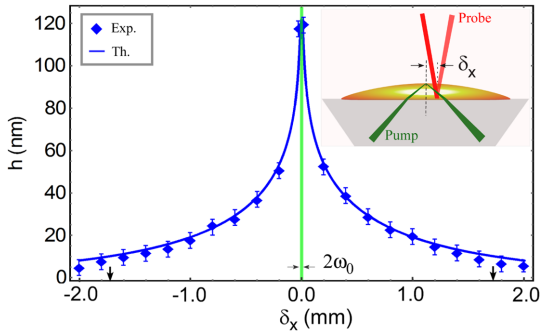

FIG. 4 (color online). Spatial profile of bulge in TIR. Inset: Schematics of the measurement with δ_x on both sides of the pump beam in plane of incidence. The capillary length is indicated by vertical arrows. The solid line is a fit with Eq. (2). Other experimental parameters are $P_0 = 2.5$ W, $2w_0 = 40$ μm, $\gamma = 30$ mN/m, and probe diameter was 750 μm.

bulge on the AW interface is one of the unique features of the radiation pressure effects near TIR.

One of the important predictions of Minkowski formalism for oblique incidence is a weak dependence of the photon momentum on the input polarization. Because of the polarization dependence of the Fresnel reflection, arising from the contrast in the refractive index at the interface, TE and TM polarizations exert different radiation pressures. However, the resulting polarization-dependent deformation for the air-water interface is nanometric (< 10 nm). Because of the high sensitivity of our technique, as shown in Fig. 3(b), we clearly resolved higher deformation in TE polarization, by around 7 nm near 47.5°, when compared with the TM polarization. This polarization-dependent deformation is obviously absent in the TIR regime. These data provide the first quantitative evidence of the unique polarization dependence of radiation-pressure-induced optofluidic deformation.

With our setup, we can easily measure the spatial profile of the bulge with nanometer precision. By keeping the pump beam fixed, we scanned the probe beams across the water drop (see inset in Fig. 4) by translating the probe mirror M (Fig. 1). Figure 4 shows our measurements of the elevation height of the bulge versus the probe position δ_x along the plane of incidence. The central region of the drop was almost flat since its size was > 10 times larger compared to the total scan range. In TIR, for spatially overlapping pump and probe beams ($\delta_x = 0$), the maximum deformation height was 120 nm for 2.5 W pump power focused to around 40 μm spot diameter. Our measurements for the deformation height for various positions of the probe show a long-range extension of the deformation. It extended more than 2 mm on each side, which was 2 orders of magnitude beyond the pump spot diameter. The capillary length of the water is indicated by vertical arrows in Fig. 4. Furthermore, the optically induced capillarylike deformation in TIR was symmetrical on both sides of the pump spot. The experimental data quantitatively agreed with the theoretical fit corresponding to Eq. (2), which uniquely determined the deformation shape.

It is worth mentioning that the maximum distance of the stationary optofluidic deformation from the excitation reported so far experimentally has been around 100 μm for soft fluid-fluid interfaces, which has also been computed with pulsed excitation under normal incidence [16,18]. Our measurements directly show that the local excitation of the AW interface in TIR has a long tail that extends much beyond previous such measurements.

The three basic characteristics of the optically produced bulge offer potential for diverse applications. First, the observed nonlinear enhancement near TIR suggests that it should be possible to create much larger deformation for a given beam by optimizing its incidence angle. Second, owing to the observed sensitivity of radiation pressure force on the laser polarization, one can actuate fluid interfaces with nanometer precision by dynamically controlling the incident polarization on an ultrafast (sub-ns) time scale. Last, the persistence of the curvature over long ranges enables a novel kind of optical traps on the air-water interface based on optically generated nN Laplace forces. Unlike conventional optical trapping, which requires direct interaction of the laser with the object, here a variety of microscopic particles (metal, dielectric, or biological) can be controlled in noncontact mode by optically manipulating the capillary curvatures in their vicinity. It should be possible to propel various objects by suitable modification of fluid interfaces with nanometric precision.

The nanometric bulge at the air-water interface near the critical angle is a generic signature due to the transfer of photon momentum. Our data validate the Minkowski model for a general incidence angle with the highest nanometric precision demonstrated thus far. Universal applicability of Minkowski momentum suggests that our results will have far reaching implications for other waves, such as for acoustic or matter waves [28].

Finally, nanometric sensitivity and ease of our technique can unravel new effects of optical forces on fast time scales with yet unexplored Bessel or vortex beams. Nonlinear optofluidic phenomenon on anisotropic fluids such as liquid-crystal droplets could also be resolved with high precision [6,29,30].

We acknowledge K. P. Yogendran for discussions and DST India for financial support.

[1] D. Psaltis, S. R. Quake, and C. Yang, Nature (London) **442**, 381 (2006).
[2] C. Monat, P. Domachuk, and B. J. Eggleton, Nat. Photonics **1**, 106 (2007).
[3] K. Campbell, A. Groisman, U. Levy, L. Pang, S. Mookherjea, D. Psaltis, and Y. Fainman, Appl. Phys. Lett. **85**, 6119 (2004).

[4] N. Bertin, H. Chraibi, R. Wunenburger, J. P. Delville, and E. Brasselet, Phys. Rev. Lett. **109**, 244304 (2012).
[5] E. Brasselet, R. Wunenburger, and J. P. Delville, Phys. Rev. Lett. **101**, 014501 (2008).
[6] A. Dogariu, S. Sukhov, and J. Saenz, Nat. Photonics **7**, 24 (2013).
[7] A. Ashkin and J. M. Dziedzic, Phys. Rev. Lett. **30**, 139 (1973).
[8] H. Minkowski, *Die Grundgleichungenfür die elektromagnetischen Vorgänge in bewegten.Nachr. Königl. Ges. Wiss. Göettingen* (1908), pp. 53–111.
[9] M. Abraham, Rend. Circ. Mat. Palermo **28**, 1 (1909).
[10] M. B. Stephen, Phys. Rev. Lett. **104**, 070401 (2010).
[11] Q. W. Cheng, W. Ding, M. R. C. Mahdy, D. Gao, T. Zhang, F. C. Cheong, A. Dogariu, Z. Wang, and C. Teck Lim, Light Sci. Appl. **4**, e278 (2015).
[12] G. B. Walker and D. G. Lahoz, Nature (London) **253**, 339 (1975).
[13] C. Baxter and R. Loudon, J. Mod. Opt. **57**, 830 (2010).
[14] R. N. C. Pfeifer, T. A. Nieminen, N. R. Heckenberg, and H. Rubinsztein-Dunlop, Rev. Mod. Phys. **79**, 1197 (2007).
[15] A. Casner and J. P. Delville, Phys. Rev. Lett. **90**, 144503 (2003).
[16] E. Brasselet and J. P. Delville, Phys. Rev. A **78**, 013835 (2008).
[17] J. P. Delville *et al.*, *Trends in Lasers and Electro-Optics Research* (NovaScience, New York, 2006), p. 158.
[18] G. C. Nelson *et al.*, Nat. Commun. **5**, 4363 (2014).
[19] F. Goos and H. Hänchen, Ann. Phys. (Berlin) **436**, 333 (1947).
[20] J. Z. Zhang and R. K. Chang, Opt. Lett. **13**, 10 (1988).
[21] I. I. Komissarova, G. V. Ostrovskaya, and E. N. Shedova, Opt. Commun. **66**, 15 (1988).
[22] O. Emile and J. Emile, Phys. Rev. Lett. **106**, 183904 (2011).
[23] E. Brasselet, Phys. Rev. Lett. **108**, 269401 (2012); O. Emile and J. Emile, Phys. Rev. Lett. **108**, 269402 (2012).
[24] G. Verma, J. Nair, and K. P. Singh, Phys. Rev. Lett. **110**, 079401 (2013); O. Emile and J. Emile, Phys. Rev. Lett. **110**, 079402 (2013).
[25] G. Verma and K. P. Singh, Appl. Phys. Lett. **104**, 244106 (2014).
[26] See Supplemental Material at http://link.aps.org/supplemental/10.1103/PhysRevLett.115.143902 for Fringe modulation by pump beam.
[27] S. Mitani and K. Sakai, Phys. Rev. E **66**, 031604 (2002).
[28] U. Leonhardt, Nature (London) **444**, 823 (2006).
[29] G. T. Molina, J. P. Torres, and L. Torner, Nat. Phys. **3**, 305 (2007).
[30] J. Chen, J. Ng, Z. Lin, and C. T. Chan, Nat. Photonics **5**, 531 (2011).